South African Statistical Journal
Vol. 59, No. 2, pp. 59–84
https://doi.org/10.37920/sasj.2025.59.2.1

Point process models for predicting the spatial distribution of rhino poaching activity in the Kruger National Park

Lisa-Ann Kirkland[1], *Inger Fabris-Rotelli*[1] *and Johan Pieter de Villiers* [2]

[1]Department of Statistics, University of Pretoria, Pretoria, South Africa
[2]Department of Electrical, Electronic and Computer Engineering, University of Pretoria, Pretoria, South Africa

Rhino poaching in South Africa continues to threaten the existence of African rhino species. Since poachers often attack wildlife parks frequently, predictive models are essential for exploiting the availability of data to gain information about the poachers. Although a number of statistical methods have been applied to poaching prediction, they either do not take the spatial variation of observations into account, require additional observational data, depend on known priors, or result in models that are overfitted and challenging to interpret. This paper proposes the use of point process models to predict the spatial distribution of poaching activity within a wildlife park. Descriptive statistics of poaching spatial point patterns have been considered, as well as univariate non-parametric kernel density estimation. However, the focus of this work is on fitting multivariate parametric point process models, using a number of environmental factors. Since real-world poaching data could not be obtained for this work, due to the sensitivity of the data, a simulation study is performed, where numerous point patterns are generated from the same underlying point process. The method can be used when no data is available, and is based on environmental preferences of poachers, which can be obtained through expert knowledge, literature reviews, or by making intelligent assumptions. The results indicate that the point process models are able to predict the initial probabilities well, for most data generating processes. Point process models thus appear to be a promising method for predicting the spatial distribution of poaching activity.

Keywords: Poaching prediction, Point process models, Rhino conservation, Simulation study.

1. Introduction

The motivation for this work is the ongoing rhinoceros (rhino) poaching crisis which may lead to the extinction of the five extant rhino species (Ferreira et al., 2022). South Africa has been hardest hit by the onslaught, with nearly 10 000 rhinos poached from 2006 to 2022 (Ferreira et al., 2022), and the situation is particularly severe in the Kruger National Park, where over 5 500 rhinos were lost due to poaching in the same period (SANParks, 2017; SADEA, 2019, 2020, 2023). The southern white rhino (*Ceratotherium simum simum*) is the most abundant species, accounting for 61% of the world's rhinos, and 72% of African rhinos, by the end of 2021 (Ferreira et al., 2022). This species is

Corresponding author: Lisa-Ann Kirkland (lisakirkland25@gmail.com)
MSC2020 subject classifications: 62H11, 62J12, 62M30

one of the greatest conservation successes, with their numbers growing from a single population of about 20 to 50 rhinos in Kwazulu-Natal in South Africa in the early 1900s, to about 21 300 animals in over 400 subpopulations by the end of 2012 (Emslie, 2020). However, their numbers have rapidly declined since then, due to high poaching rates. The actual poaching rates for white rhino in the Kruger National Park were on average 10 to 12% of the population per annum from 2014 to 2017, which is larger than the estimated maximum growth rate of 9% for white rhino (Emslie et al., 2018). By the end of 2022, there were about 1 850 white rhinos remaining in the Kruger National Park, an 82% decrease in their population since 2012 (SANParks, 2023; Ferreira et al., 2015). While the white rhino population in the Kruger National Park was affected by the drought during the 2015/2016 wet season, poaching is the largest contributor towards the population decline (Ferreira et al., 2019). At current poaching rates, the southern white rhino is predicted to go extinct within the next two decades (Di Minin et al., 2015).

Rhino poaching is a multifaceted international problem, involving criminal syndicates in the illegal wildlife trade, low public awareness and education about the supposed medicinal effects of rhino horn in Asian countries, and poverty-stricken communities living near the wildlife parks in South Africa and neighbouring countries (Jooste and Park, 2022). Addressing the problem thus entails utilising multiple solutions, but includes anti-poaching ground operations since the rangers in the park are the last line of defence to protect these silent victims (Ferreira et al., 2015; Lemieux, 2014). Poachers often conduct frequent attacks on wildlife parks (Fang et al., 2015), allowing the rangers to gather observational data of poaching activities, such as poached animal carcasses, arrests, snares, tracks, and camps. Furthermore, poachers often return to sites of past success (Kar et al., 2015), so historical data could assist in predicting current poaching trends. Predictive models are therefore very important for estimating high risk poaching areas. However, publishing results of poaching analyses on real-world data remains problematic, since poachers can also gain access to this information and their behaviour may be influenced by it. Particularly, the severity of the rhino poaching status in the Kruger National Park called for a strict policy of non-disclosure. For some time, even the numbers of poached rhinos were withheld from publication, and tourists were (and still are) discouraged from sharing the locations of their rhino sightings.

A number of statistical methods have been proposed for predicting the probability of poaching activities in a given region. Some general methods have been utilised, including classification methods such as k-nearest neighbours, support vector machines, and AdaBoost (Park et al., 2015), as well as regression methods such as multiple linear and polynomial regression, Gaussian process regression, support vector regression (Park et al., 2015), and logistic regression (Subedi and Subedi, 2017). While these methods perform reasonably well, better estimates could be obtained by considering the spatial variation in the occurrences of poaching activities, and any possible spatial dependence between them. To account for spatial correlation, Rashidi et al. (2015) explore various clustering methods, including Kulldorff's spatial scan statistic (Kulldorff, 1997), the flexible spatial scan statistic (Tango and Takahashi, 2005), and the spatio-temporal scan statistic (Kulldorff et al., 2005), while Lemieux et al. (2014) propose using spatial autocovariate Poisson regression. However, these models require more data than the locations of poaching activities: animal population data is needed for the clustering methods, and ranger patrol data is necessary for autocovariate Poisson regression. Other work in the field propose using spatial regression models within a Bayesian framework (Rashidi et al., 2016, 2018; Beale et al., 2018), and the use of Bayesian networks (Koen et al., 2014, 2017;

Gatsheni, 2019), but these models require that priors on the parameters be obtained through expert knowledge. Finally, ecological models of occupancy (Critchlow et al., 2015; Ferreguetti et al., 2018; de Matos Dias et al., 2020; Ghoddousi et al., 2022) and species distribution (Kuiper et al., 2020) have been applied to the poaching problem. Both methods require data for presence and absence of poaching activities, with occupancy models requiring repeat observations at each site (Jha et al., 2022). Furthermore, both methods result in complicated and/or uninterpretable models: the Bayesian hierarchical occupancy model (Critchlow et al., 2015) consists of three layers and depends on known priors, while the species distribution model (Kuiper et al., 2020) consists of an ensemble of various methods including generalised linear models, generalised additive models, and multivariate adaptive regression splines, maximum entropy, artificial neural networks, boosted regression trees, and random forests.

The goal of this work is to examine the use of spatial point process models (Baddeley et al., 2015) to predict poaching locations. The models are simple and interpretable, require only the locations of detected poaching activities and make few assumptions about their distribution, yet flexible enough to incorporate other types of data that might be available, such as animal population and ranger patrol data. There has been some interest in using spatial point pattern analysis for poaching prediction. Rifaie et al. (2015) discuss a number of descriptive statistics, but do not take account of correlations with environmental factors. Shaffer and Bishop (2016) take the same approach, but also consider univariate effects of some environmental factors on non-parametric kernel density estimates of poaching intensity. However, the focus of this work is to fit multivariate parametric point process models to explain the spatial variation in the intensity of poaching activities using environmental factors as explanatory variables. While such models have been used to understand how environmental factors influence animal population distributions (MacFadyen et al., 2019), to our knowledge these models have not been applied to the poaching problem.

There are two main objectives in this paper. One of the major difficulties of studying rhino poaching in South Africa, and particularly in the Kruger National Park, is the inability to obtain real-world poaching data due to the extreme sensitive nature of the data. The first objective thus entails dealing with situations where poaching data has not been collected or is not available for analysis. A heuristic method is proposed to calculate poacher probabilities within the study region, based on environmental preferences of the poachers. These preferences can be obtained from expert knowledge of poacher behaviour in the region, but intelligent assumptions can be made if such information is not available. If poaching data is available, the second objective is to fit a probability model, using environmental factors to explain the spatial variation of poaching activities in the region. A simulation study is presented to analyse the properties of model estimates and predictions. However, since real-world poaching data is not available for this study, the Poisson point process is used to generate point patterns that represent detected occurrences of poaching activities, based on the probabilities that are calculated using the heuristic method. If a model can be fitted to a large number of such generated point patterns, and consistently makes good predictions of the original probabilities, then it follows that the methodology should work on real-world data, if such data were available.

The data and methods used in this paper are described in Section 2, details regarding calculations are given in Section 3, and the results of the simulation study are presented in Section 4, followed by a discussion of the results and point process models in Section 5. Finally, some concluding remarks and suggestions for further research are provided in Section 6.

2. Materials and methods

2.1 Study region

The Kruger National Park covers a vast region, of almost 20 000 km^2, in the north-east of South Africa, in the Limpopo and Mpumalanga provinces. The park extends 350 km long from north to south, has an average of 60 km wide from east to west (Cromsigt and te Beest, 2014), and a perimeter of about 1 000 km (Jooste and Park, 2022). The natural boundaries of the park are the Limpopo and Luvuvhu rivers in the north, the Crocodile and Nsikazi rivers in the south, and the 800 km Lebombo mountain range in the east. More information about the Kruger National Park is summarised in Kirkland (2023), such as climate, average rainfall, main landscape types, and the formation of the the Great Limpopo Transfrontier Park (GLTP) and Greater Lebombo Conservancy (GLC). The GLTP is shown in the left panel of Figure 1, along with the private land adjacent to the Kruger National Park on the west and the GLC to the right of the park (data provided by PPF (2023)). The position in Africa is also shown. The four regions of main landscape types are shown in the middle panel of Figure 1, as well as the rivers (blue) and mountains (brown) that form natural boundaries of the park. A smaller study region is selected for the analysis, bound between 31.3° and 32.05° longitude, and between -24.75° and -24.35° latitude. The region is indicated by a cyan rectangular region in the right panel of Figure 1, overlaid onto a terrain background map of the surrounding area.

2.2 Spatial covariates

Environmental factors for the Kruger National Park are extracted from the public shapefiles available in the SANParks data repository (SANParks, 2020). Table 1 provides a description of the shapefiles that are used for each environmental factor, as well as the type of spatial geometries. The environmental factors for the specified study region in the Kruger National Park are shown in Figure 2, where the region contains one public gate, three main roads, two main camps and two picnic spots.

Table 1. Environmental factors derived from SANParks public shapefiles.

Shapefile	Geometry	Feature	Subset
bndry_kruger.shp	Polygons	Park boundary	
geology.shp	Polygons	Dense trees	DOMWOODY field contains "dense savanna" or "forest"
		Steep mountains	GEOMORPH field contains "strongly undulating" or "intensely dissected"
roads_tarred_public.shp	Lines	Tarred roads	
rivers_main.shp	Lines	Main rivers	
water_dams_geo.shp	Points	Dams	
springs.shp	Points	Water holes, fountains & drinking troughs	
water_holes.shp	Points		
drinking_trough.shp	Points		
camps_main.shp	Points	Main camps	
picnic_spots.shp	Points	Picnic spots	
gates_public.shp	Points	Public gates	

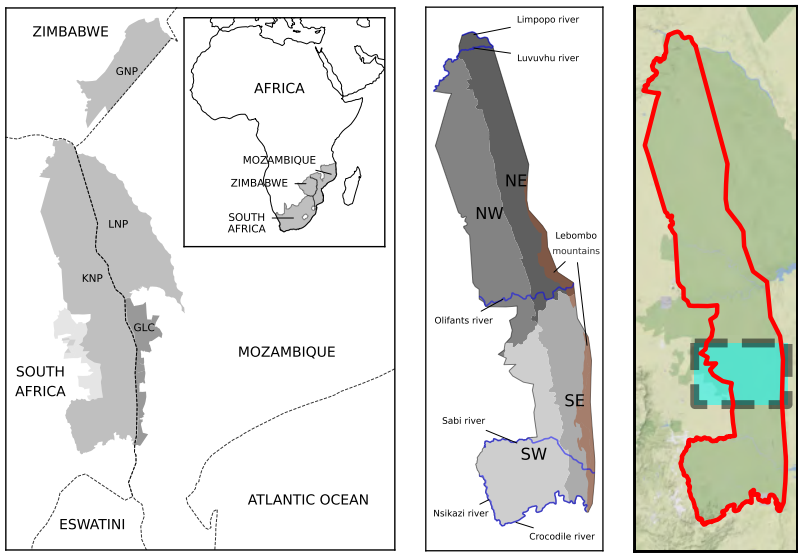

Figure 1. *Left*: Map showing the GLTP (medium grey), the GLC (dark grey), and private parks (light grey). *Middle*: Regions with nearly homogeneous landscapes and the natural boundaries, including rivers (blue) and mountains (brown). *Right*: Smaller study region (cyan).

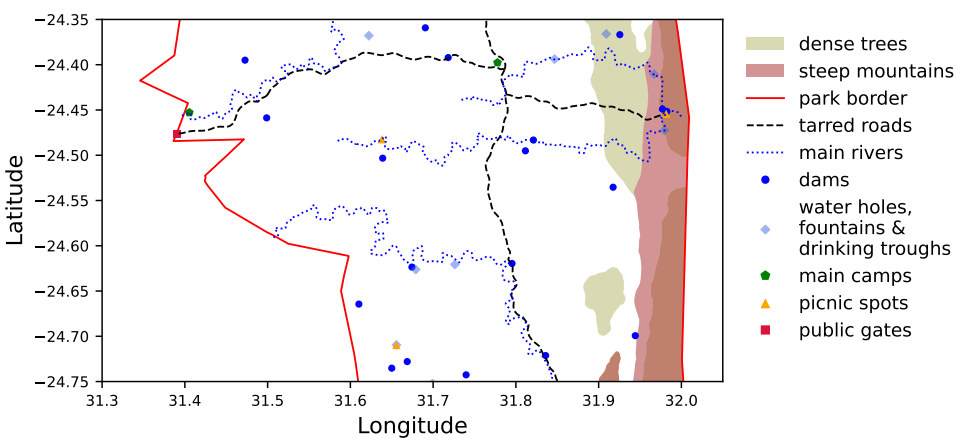

Figure 2. Map of environmental factors in the study region.

To perform the analysis, the study region is divided into a grid of cells, where each cell is 1×1 km in size. The size of the grid cells is chosen so that the area of one cell is small enough to ensure a high probability of arrest when the rangers are in the same cell as the poachers. Ideally, the size of grid cells must correspond with anti-poaching ground operations. If this information is unknown, 1×1 km cells can be used for simplicity. The grid contains 77×44 =3 388 cells in total. In Figure 3, an illustrative example is shown where the poachers are restricted to stay within a home base, defined by a circular area within the study region. Furthermore, it is assumed that it is the wet season, and the poachers are restricted from entering cells with rivers and dams. After these cells are excluded, there are 2 245 cells which can be accessed by the poachers.

Spatial covariates are created for some of the environmental factors, including roads, camps, picnic spots, gates, border, dams, and water sources. Consider an environmental factor denoted by points, such as camps. Let c_1 and c_2 be the locations of the two camps in the study region. For each grid cell, the Euclidean distance is calculated from the cell centroid to the nearest camp. Suppose the cell centroid is at location u, then this distance is given by $d(u) = min\{D(u, c_1), D(u, c_2)\}$, where $D(u, c_i)$ is the Euclidean distance between the point u and the point c_i. For example, if c_1 is closer to the point u than c_2, then $d(u)$ is the Euclidean distance between c_1 and u. Distances are calculated similarly for an environmental factor denoted by lines, such as roads. For example, let r_1 be the point along the first river that is closest to u. Similarly, let r_2 and r_3 be the points along the other two rivers that are closest to u. Then $d(u) = min\{D(u, r_1), D(u, r_2), D(u, r_3)\}$.

Images of these spatial covariates are included in Figure 4. The distances in kilometers are indicated by a colour scale, where low values are blue and high values are yellow.

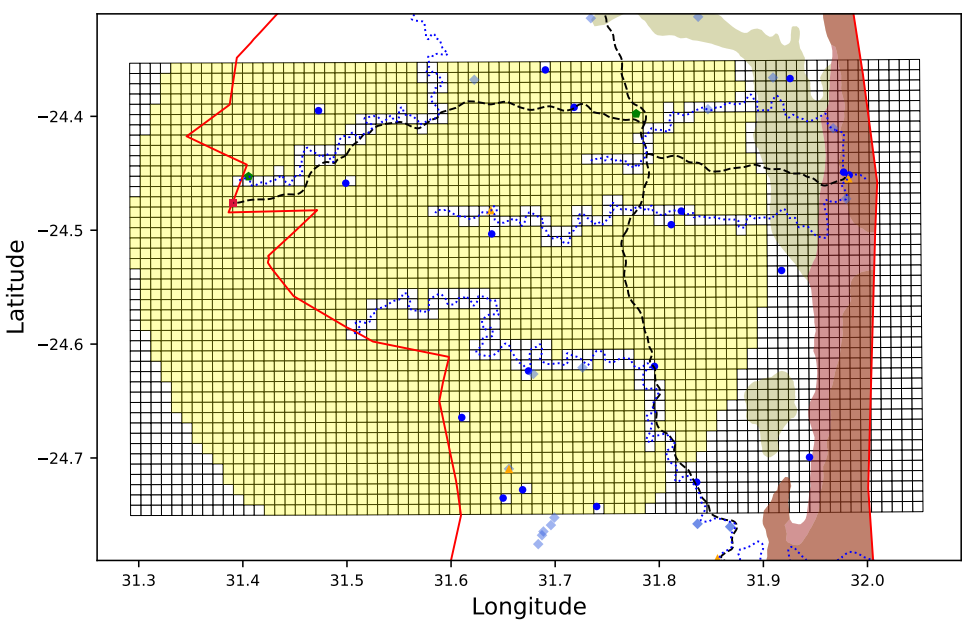

Figure 3. Grid over the study region containing 3 388 cells of size 1×1 km. Poachers can access the 2 245 yellow-shaded cells.

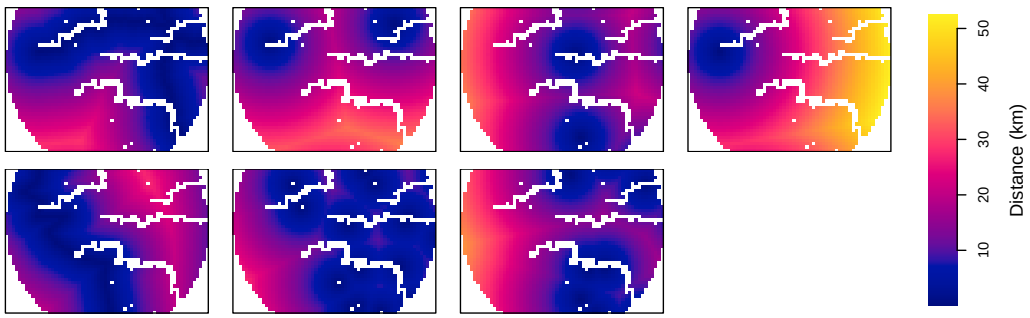

Figure 4. Spatial covariates in the study region. *Top (left to right):* distances to roads, camps, picnic spots, and gates. *Bottom (left to right):* distances to the border, dams, and water sources.

2.3 Simulated poaching data

The poaching data consists of global positioning system (GPS) coordinates for locations where poaching activity is detected in the study region, over a specific period of time. Detection of poaching activities, such as poacher tracks, snares, crossings, sightings, and camps, can be more difficult to detect than poached carcasses. Aerial photographs are utilised to detect poached carcasses (Ferreira et al., 2015), but other poaching activities are obtained via field methods and recorded in ranger logbooks (Ghoddousi et al., 2022). As the rangers patrol the area, they record the location and type of poaching activity whenever signs of poachers are detected. Poaching observations are thus dependent on where the rangers patrol. Obviously rangers cannot make observations in areas where they have not patrolled, but imperfect detection is also likely in areas where they have patrolled, since some signs (such as tracks, fence openings and snares) are very well hidden by the poachers (Gholami, 2018). Although the detection of points is unreliable, the analysis can be performed explicitly on the process of detected points (Baddeley et al., 2015).

To address cases where poaching data is not available, a heuristic method is presented to calculate a probability distribution for poaching activity across all the cells in the grid. The method is derived by setting some rules that were determined by trial and error. Poacher preferences for different environmental factors form the basis for these rules. Environmental factors are important elements of poaching opportunity structures, since roads and the border provide access points to poachers and water sources attract rhinos (Eloff and Lemieux, 2014). This information is used to determine which regions poachers would prefer over others. If there is no prior knowledge of poacher behaviour in the study region, then intelligent assumptions can be made, or the literature can be consulted for past findings. Unfortunately, details of rhino poaching in the Kruger National Park are rarely published, due to the extreme sensitivity around poaching information in the park. This led to difficulties in obtaining expert knowledge from the literature. However, some findings are presented by Eloff and Lemieux (2014) (albeit a small study), and Jooste and Park (2022) provide a first-hand account of anti-poaching operations in the Kruger National Park. The spatial trends of rhino poaching described in these works are listed below.

- Rhino poaching predominantly occurs in the southern region of park, with moderate levels of poaching in the central region (Eloff and Lemieux, 2014).
- After infiltrating the border, poachers can easily walk about 25 km into the park before setting up makeshift camps to observe, often near water (Jooste and Park, 2022).
- Poachers sometimes enter the park in vehicles, using the staff and tourist facilities, and get dropped off deep into the park (Jooste and Park, 2022).
- Nearly half of poaching incidents occur within 5 km of the border, mostly 2-3 km, and most of these incidents are along the eastern border that the park shares with Mozambique (Eloff and Lemieux, 2014).
- Most poaching incidents occur within 2.5 km from the road (Eloff and Lemieux, 2014).

Since findings of poacher behaviour in the Kruger National Park (KNP) are limited, some assumptions of their preferences are made, taking the literature into account where possible. Two types of poacher preferences are considered: avoidant features are environmental factors that could increase their risk of capture; while favourable features are environmental factors that provide access or aid in finding rhinos. For example: poachers would probably like to avoid any park entrance gates since rangers often conduct searches there; they would also avoid main roads, camps and picnic spots to prevent being identified by the public; they might favour staying near to the park border to make escape easier; and they would probably favour being near to water sources since it is likely that they might find wildlife there. While Eloff and Lemieux (2014) report that poaching incidents occur near to the roads, it is assumed that they are referring to the numerous small dirt roads within the park, not the main roads used in this study. Note also that Eloff and Lemieux (2014) conduct their analysis on poached carcasses only, and exclude other signs of poaching activities.

To formulate rules from the poacher preferences, a distance d is specified for each environmental factor, and a weight is then calculated for each grid cell. The weight in a cell can be interpreted as the cell's relative importance score for the environmental factor. Cells start with a weight of 0.5 to indicate indifference for that cell. For an avoidant feature, the distance d refers to how far poachers want to stay away from the feature, and the weight for a cell is decreased if the cell is within d km from the nearest feature. That is, the weight $w(u)$ for a cell with centroid at location u is given by

$$w(u) = \begin{cases} 0.5 \times \left(1 - \frac{d - d(u)}{d}\right) & \text{if } d(u) \leq d \\ 0.5 & \text{if } d(u) > d, \end{cases} \tag{1}$$

where $d(u)$ is the distance from the cell centroid to the nearest feature, as defined in Section 2.2. For a favourable feature, the distance d refers to how near poachers want to stay to the feature, and the weight for a cell is increased if the cell is within d km from the nearest feature. That is, the weight $w(u)$ is given by

$$w(u) = \begin{cases} 0.5 \times \left(1 + \frac{d - d(u)}{d}\right) & \text{if } d(u) \leq d \\ 0.5 & \text{if } d(u) > d. \end{cases} \tag{2}$$

Table 2. Assumptions of the poachers' environmental preferences.

Environmental feature	Avoid	Favour
Roads	5 km	
Camps	8 km	
Picnic spots	8 km	
Gates	10 km	
Border		30 km
Dams		25 km
Water sources		20 km

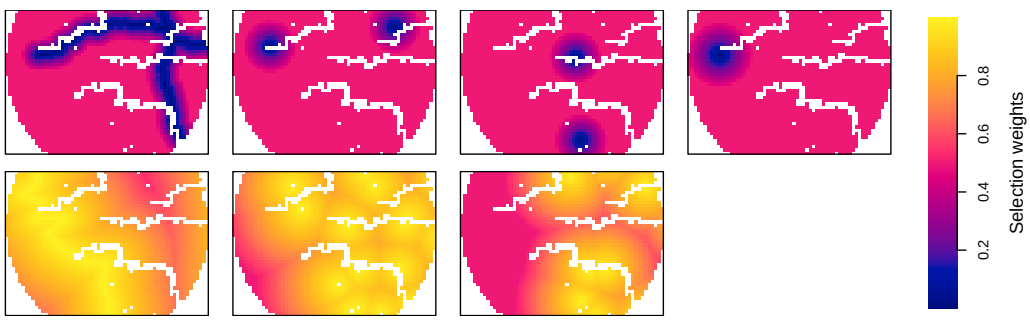

Figure 5. Heuristic weights in the study region. *Top (left to right):* distances to roads, camps, picnic spots, and gates. *Bottom (left to right):* distances to the border, dams, and water sources.

The assumptions made about the environmental preferences of the poachers are summarised in Table 2, including how far to stay away from avoidant features, and how near to stay to favourable features. For each feature, the weights are calculated in every cell, but only cells that are within the distance range are affected by the feature. For example: for an avoidant feature such as roads, weights are decreased within 5 km of roads but are unchanged for cells further than 5 km; and for a favourable feature such as water, weights are increased for cells within 20 km of water but are unchanged for cells further away. Thus, each feature has a conditional effect on the cells, since it depends on the specified distance range.

The weights for each of the environmental factors are shown in Figure 5. The weights are indicated by a colour scale, where low values are blue and high values are yellow. Avoidant features are shown in the top row, where $w = 0.5$ for all cells greater than d km from the feature, and $w < 0.5$ for all cells within d km of the feature. Favoured features are shown in the bottom row, where $w = 0.5$ for all cells greater than d km from the feature, and $w > 0.5$ for all cells within d km of the feature.

To calculate probabilities that take all of the poacher preferences into account, the cell weights for each of the environmental factors are multiplied with each other. These values are then normalised over the entire grid to form a probability distribution. These values are referred to as heuristic poacher probabilities, and are shown in Figure 6, with low values in blue and high values in yellow.

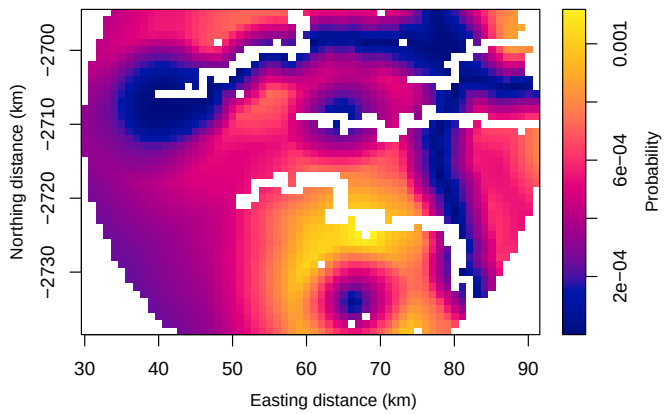

Figure 6. Heuristic poacher probabilities in the study region.

2.4 Spatial point process models

This paper proposes using spatial point process models to predict poaching locations. Spatial point patterns consist of an observation window and a number of points distributed in some way within the observation window. The observation window is an important component of a spatial point pattern dataset, since it is necessary to know where points are not observed. The method can be applied to poaching datasets since the study region forms an observational window and the GPS locations of detected poaching activities can be plotted as points in the study region. The analysis of a point pattern is focused on the spatial arrangement of points, so there is information in open spaces between the points, where points are not observed, as well as where points are observed (Baddeley et al., 2015; Diggle, 2013). There are two main properties that are of interest when studying point patterns: the intensity of the points and the interaction between the points. The intensity is the expected density of points per unit area, and the inter-point interaction is the stochastic dependence between points (Baddeley et al., 2015). The intensity will be the focus in this paper. A statistical analysis of a point pattern can provide answers pertaining to spatial trends in the density of points, such as whether the density depends on spatial covariates, and whether the points are spread uniformly in the region. The aim is not to answer questions about the points themselves, but rather about the way in which the points are generated. A spatial point process is a random mechanism that generates a point pattern, and an observed point pattern is a sample, or realisation, of a random point process (Baddeley et al., 2015; Illian et al., 2007). A random point process $\mathbf{X} = \{X_1, X_2, \ldots, X_n\}$ is a homogeneous Poisson point process, with constant intensity $\lambda > 0$, if

- the expected number of points in a region B is given by $\mu_B = \lambda|B|$, where $|B|$ is the area of region B,
- the number of points in any disjoint regions are independent random variables, and
- the number of points in any region B, denoted by $N(\mathbf{X} \cap B)$, has the Poisson distribution with probability mass function

$$P(N(\mathbf{X} \cap B) = k) = \frac{e^{-\mu_B}\mu_B^k}{k!}, \tag{3}$$

where $k \in \mathbb{N}_0$ and $\mu_B = \lambda|B|$.

For an inhomogeneous Poisson process, the intensity is spatially varying $\lambda(u)$, and the expected number of points in a region B is given by

$$E(N(\mathbf{X} \cap B)) = \mu_B = \int_B \lambda(u)du. \tag{4}$$

The homogeneous Poisson process is completely random: the points have no preference for location and the number of points is random. The points are spatially independent since the number of points in a region B is independent of the number of points in the complement of B. The process is called complete spatial randomness (CSR). In this paper, CSR is used as the null model to compare whether the inhomogeneous Poisson model provides a better fit. For the inhomogeneous Poisson process, the number of points are random and there is spatial independence between the points, but the points have a preference for certain locations. The intensity function, $\lambda(u)$, varies by location, and is the expected number of points per unit area at location u. The Poisson point process model explains the spatial variation in the intensities of the point pattern over the study region, given the spatial covariates. The model takes the log-linear form and is given by (Baddeley et al., 2015),

$$\log(\lambda(u)) = \sum_{j=1}^{p} \theta_j Z_j(u), \tag{5}$$

where θ_j are parameters to be estimated, and Z_j for $j = 1, \ldots, p$ are the spatial covariates given by the distances to roads, camps, picnic spots, gates, the border, dams, and water sources.

Suppose that observed poaching data is available, and provided as GPS locations of detected poaching activities, within a study region over a specific period of time. The data can be represented as a spatial point pattern in the region, which is assumed to be a realisation of an inhomogeneous Poisson point process with spatially varying intensity $\lambda(u)$. We propose fitting the parametric Poisson point process model to explain the variation in the intensity of poaching activities over the region, using spatial covariates of environmental factors as explanatory variables.

3. Model development and evaluation

The spatial analysis is performed in R 4.2.3 (R Core Team, 2023), using the `spatstat` package (Baddeley and Turner, 2005). Due to the sensitive nature of real-world poaching data, the inhomogeneous Poisson point process will be used to generate poaching data. An observed poaching dataset can be seen as one realisation of a Poisson point process with intensity $\lambda(u)$. Suppose that an assumed $\lambda(u)$ is a good approximation for the true intensity, then the simulation study generates a new realisation from the same Poisson point process at every iteration of the study.

The heuristic poacher probabilities calculated in Section 2.3 are used as a basis for the simulated data. An inhomogeneous Poisson point pattern is generated in the study region W. By the conditional property, given that the expected number of points is μ_W, the points have the same probability

distribution over the window, with probability density $f(u) = \lambda(u)/\mu_W$, where $\mu_W = \int_W \lambda(u)du$. Suppose the assumption is made that $\mu_W = 500$, then the intensity can be calculated as $\lambda(u) = 500f(u)$, where $f(u)$ is given by the heuristic poacher probabilities. The resulting intensity image has mean 0.222, and the integral over the region is 500. An inhomogeneous Poisson point pattern is generated using this intensity image. The point pattern generated from the image has 487 points in the point pattern and the average intensity is 0.217 points per km^2, which corresponds with the intensity image. Assuming that we start with a good approximation of the true poacher probabilities and reasonable number of points in the region, the generated point pattern should be a good representation of a real-world poaching dataset. Varying sample sizes will be tested in the simulation study, to determine the minimum required number of points needed for analysis. When using real-world data, the specified period of data collection can be extended until enough points are observed in the region.

A homogeneous Poisson point pattern is generated in the study region W for comparison. Assuming that $\mu_W = 500$, by the conditional property, the constant intensity is calculated as $\lambda = \mu_W/|W| = 500/2245 = 0.223$, where $|W| = 2245$ is the total area of the study region. There are 498 points in the generated point pattern and the average intensity is 0.222 points per km^2. The homogeneous point pattern is shown in the left panel of Figure 7. The right panel shows the inhomogeneous point pattern overlaid onto the spatially varying intensity image, where the intensity is indicated by a colour scale with low values in blue and high values in yellow. A higher density of points is apparent in the yellow regions, where the intensity is higher, and almost no points occur in the blue regions, where the intensity is close to zero.

Data is also generated using window sampling, to assess whether a model fitted to data in a smaller window is able to make good predictions in the larger window. Window sampling assumes that points are bounded by some larger region but that observations are confined to a specific study region (Baddeley et al., 2015). When the wildlife park is very large, it may be infeasible to collect data in the entire region, since data collection can be costly when conducting aerial surveys, or very time consuming when using field methods. A smaller study region may thus be more plausible. If an inhomogeneous Poisson process is assumed, the number of points in any disjoint regions are independent random variables, and by definition, these counts have a Poisson distribution. Thus, if a smaller region B of the wildlife park is chosen as the study region, the point pattern observed

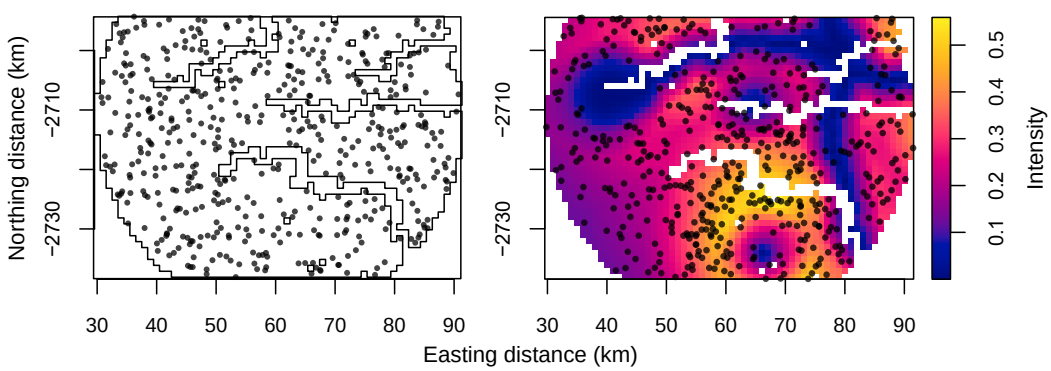

Figure 7. *Left:* Homogeneous Poisson point pattern in the window W. *Right:* Inhomogeneous Poisson point pattern in the window W, and the intensity image used to generate the points.

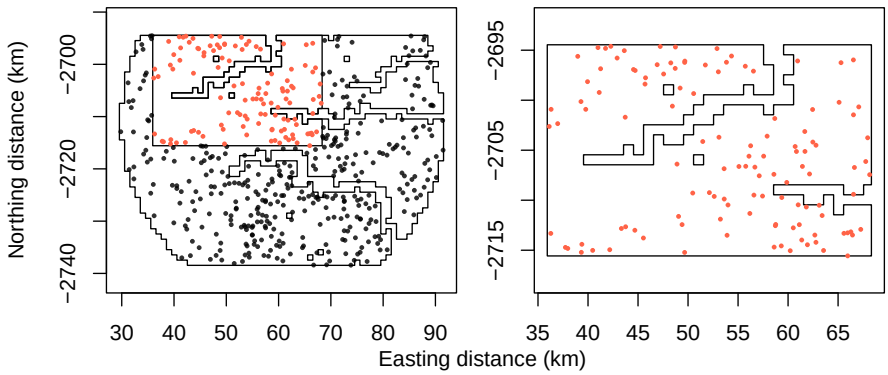

Figure 8. *Left:* Inhomogeneous Poisson point pattern in the window W and position of the smaller window B. *Right:* The sampled point pattern in the smaller window B.

inside B should also be a Poisson process. Selecting the sampling window inside the wildlife park can be done using probability sampling or simply by selecting a feasible region which is assumed to be representative of the larger park (Diggle, 2013). The size of the sampling window should be large enough so that all essential information is in the window. Figure 8 shows a smaller observation window B and its position within the larger study region W, in the left panel. The areas of each region are $|W|$ =2 245 km^2 and $|B|$=624 km^2. The point pattern in the figure is the inhomogeneous Poisson point pattern shown in the right panel of Figure 7, consisting of 487 points. The points from this pattern that are sampled in the smaller window B are shown in the right panel of Figure 8. The sampled point pattern is obtained by selecting the subset of points in B. There are 119 points in the point pattern and the average intensity is 0.191 points per km^2.

Finally data is generated using various random thinning methods. Random thinning is a process in which points in a point pattern are randomly deleted based on some retention probability (Illian et al., 2007). For example, a point pattern of wildlife animal herds is naturally thinned due to animal mortality. Thinning can also be used to obtain a smaller sample of the dataset, or to account for different levels of detection error. Here thinning is used on simulated data to generate a more realistic dataset which accounts for poaching activity that goes undetected in the wildlife park. The analysis is conducted on the process of detected poaching activities, so a realisation of this process should be equivalent to thinning a point pattern of all poaching activities, since a large proportion of poaching activities are likely to go undetected. Independent thinning is where points are deleted or retained, regardless of the fate of other points (Baddeley et al., 2015). Illian et al. (2007) describe three different types of independent thinning:

- *p-thinning*

  Each point is deleted with probability $1 - p$. The retention probability p is constant, and deletion of a point is independent of its location.

- *$p(u)$-thinning*

  The retention probability is a deterministic function $p(u)$ with $0 \leq p(u) \leq 1$, and deletion of a point is dependent on location.

- *$P(u)$-thinning*

  Thinning is based on a random field $P(u)$, with values in $[0, 1]$, which is independent of the original process. That is, $P(u)$ is a random variable. Suppose that $p_1(u)$ is one realisation of $P(u)$, then $p_1(u)$-thinning is applied to the original process. This might seem equivalent to $p(u)$-thinning. However, another realisation of $P(u)$ might be observed in future analyses.

If $\lambda(u)$ is the intensity function of the original process, then the intensity of the thinned process is $\tau(u) = p(u)\lambda(u)$, where $\lambda(u) = \lambda \forall u$ if the original process is homogeneous, $p(u) = p \forall u$ if the process is p-thinned, and $p(u) = E(P(u))$ if the process is $P(u)$-thinned. If the original process is a Poisson process, the $p(u)$-thinned process is an inhomogeneous Poisson process, and the $P(u)$-thinned process is a doubly stochastic Poisson process (or Cox process). Cox processes (Cox, 1955) are modified Poisson processes in which the intensity is random, known as the driving intensity.

Suppose that the heuristic poacher probabilities (Figure 6) form a spatially varying retention function, proportionally scaled in an attempt to achieve a mean value of 0.5, for comparison with the p-thinned process. The image is shown in the left panel of 9. This image is used to apply $p(u)$-thinning to a homogeneous Poisson point process. This case is similar to a scenario where the rangers are more likely to detect poaching activity in some areas than in others. For example, grassland areas with fewer trees have better visibility. The benefit of simulating data in this way is that the underlying process could be a homogeneous or inhomogeneous Poisson process. The homogeneous point process is used here to demonstrate that the resulting $p(u)$-thinned process is indeed inhomogeneous. Lastly, $P(u)$-thinning is applied to a homogeneous Poisson point process by adding random noise to the retention probability function and then rescaling. This probability image is shown in the right panel of Figure 9. This is analogous to some random occurrence influencing the detection probability. For example, heavy rains could make it difficult to detect poacher tracks in the mud. The retention probability image on the left is fixed, while the image on the right contains a random effect and this is just one realisation of the random process.

The process is demonstrated for $p(u)$-thinning of the homogeneous Poisson (CSR) point pattern, shown in the left panel of Figure 7. Figure 10 is a depiction of the thinning operation. The CSR point pattern is shown in the left panel and has 498 points and average intensity of 0.222 points per km^2.

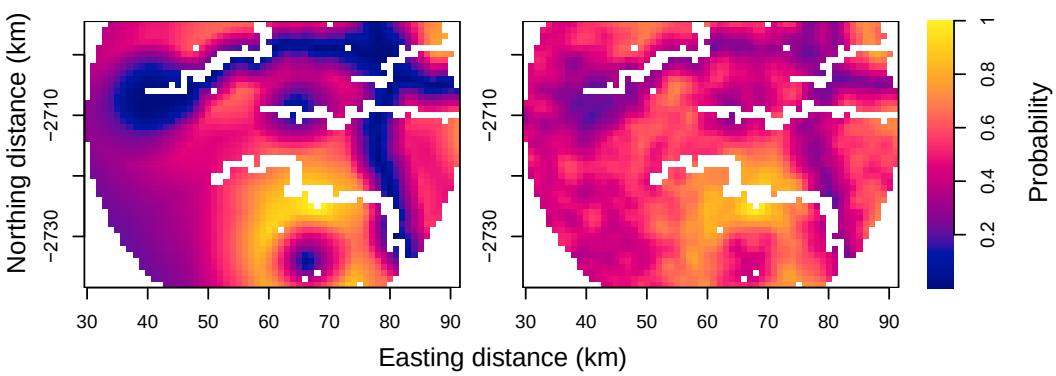

Figure 9. Retention probability functions for independent thinning. *Left:* $p(u)$-thinning. *Right:* One realisation of $P(u)$-thinning.

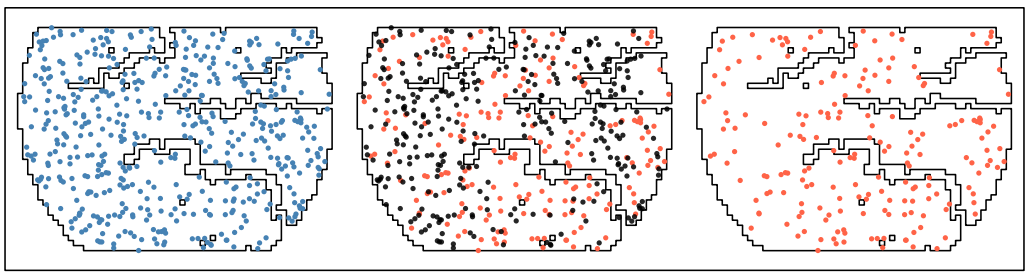

Figure 10. Independent $p(u)$-thinning applied to CSR process. *Left:* CSR point pattern (blue). *Middle:* Deleted points (black) and retained points (red). *Right:* Thinned point pattern.

The deleted points are shown in black in the centre panel. The right panel is the thinned point pattern, which is an inhomogeneous Poisson pattern, it has 190 points and an average intensity of 0.085 points per km^2.

A simulation study is performed to assess how well the Poisson model can estimate the intensity when fitted to different simulated point processes. The data is generated for the following point processes: homogeneous Poisson process, inhomogeneous Poisson process, window sampling of an inhomogeneous Poisson process, p-thinning of an inhomogeneous Poisson process, $p(u)$-thinning and $P(u)$-thinning of a homogeneous Poisson process. The points are generated in the large window W, and the smaller region B is used for window sampling. Another concern is how large the sample size should be for an adequate analysis, and if the estimates are consistent. The expected number of points μ is assumed to be the sample size, which is set to vary in $\{50, 100, 200, 300, 400, 500, 1000, 5000\}$. For comparison purposes, the sample size should be the same for all the processes.

For the homogeneous Poisson, $\lambda = \mu_W/|W|$. For the inhomogeneous Poisson, $\lambda(u) = f(u)\mu_W$, where $f(u)$ is given by the heuristic poacher probabilities. For window sampling, the probability of a point falling in the sampling window is set to $q = 0.8|B|/|W|$. The sample size needed for W is then calculated as $\eta = \lfloor \mu_W/q \rfloor$. The points are generated as before, with λ calculated using η instead of μ_W. The point pattern is then sampled by the window B, which should have expected sample size μ_B. A similar process is followed for thinning, the sample size needed for the initial process η is calculated first, based on what the sample size of the thinned process should be, and λ is calculated using η. For p-thinning, the retention probability is $p = 0.5$ and $\eta = \lfloor \mu_W/p \rfloor$. For $p(u)$-thinning, the retention probability is calculated as $p(u) = 0.5f(u)/\bar{f}(u)$, where $\bar{f}(u)$ is the mean of $f(u)$, and then divided by $\max(p(u))$ to ensure values in $[0, 1]$. Then $\eta = \lfloor \mu_W/p(u) \rfloor$. Lastly, for $P(u)$-thinning, the process is the same as for $p(u)$-thinning except that random noise is added when calculating the retention probability. The random noise, denoted by ϵ, is generated in $|W|$ as a uniform random variable in the range $[0, 0.5]$ and then smoothed using an isotropic Gaussian kernel with $\sigma = 1$. Then the retention probability is $P(u) = 0.25f(u)/\bar{f}(u) + \epsilon$, and as before, divided by $\max(P(u))$ to ensure values in $[0, 1]$. A new realisation of ϵ is generated for each iteration of the simulations to ensure that $P(u)$ is a random variable. Generating the data in these ways, the heuristic poacher probabilities $f(u)$ are used in every process (except for the homogeneous Poisson process), either to calculate the intensity or the retention probability. The input parameters are summarised in Table 3.

Simulations are run to generate 1 000 point patterns for each process, and Poisson models are fitted

Table 3. Input parameters for generating point patterns with varying sample size.

Process	Sample Size	Intensity	Retention Probability
Homogeneous Poisson	μ_W	$\mu_W/\lvert W\rvert$	
Inhomogeneous Poisson	μ_W	$f(u)\mu_W$	
Window of inhomogeneous Poisson	$\eta = \lfloor \mu_W/q \rfloor$	$f(u)\eta$	$q = 0.8\lvert B\rvert/\lvert W\rvert$
p-Thinning of inhomogeneous Poisson	$\eta = \lfloor \mu_W/p \rfloor$	$f(u)\eta$	$p = 0.5$
$p(u)$-Thinning of homogeneous Poisson	$\eta = \lfloor \mu_W/p(u) \rfloor$	$\eta/\lvert W\rvert$	$p(u) = \frac{0.5f(u)/\bar{f}(u)}{\max[0.5f(u)/\bar{f}(u)]}$
$P(u)$-Thinning of homogeneous Poisson	$\eta = \lfloor \mu_W/P(u) \rfloor$	$\eta/\lvert W\rvert$	$P(u) = \frac{0.25f(u)/\bar{f}(u) + \epsilon}{\max[0.25f(u)/\bar{f}(u) + \epsilon]}$

to the data. The homogeneous Poisson (CSR) model is fitted as the null model, that is $\log \lambda = \theta$. Then the inhomogeneous Poisson model is fitted with the covariates distances to roads, camps, picnic spots, gates, border, dams and watering holes. Since the heuristic poacher probabilities are calculated using all of these environmental factors, and the intensity is proportional to the probability, it is reasonable to assume that the full covariate model would provide an adequate fit of the intensity. This model takes the form in (5). The point process residual for the region W is given by

$$\mathcal{R}(W) = N(\mathbf{x} \cap W) - \int_W \hat{\lambda}(u)du, \tag{6}$$

where $N(\mathbf{x} \cap W)$ is the number of points in the point pattern $\mathbf{x}$ within the region W, and $\hat{\lambda}(u)$ is the estimated intensity from the model.

The point process residual has a different geometrical interpretation to normal regression analysis. For regression, the observed values and the estimated values are points in space. However, for point processes, the observed values are points in space but the estimated values represent the intensities in each grid cell. Baddeley et al. (2015) describes the residual measure, by analogy, as a spatial distribution of electric charge. Suppose the data points each carry a positive charge of 1 unit, and the background space has $\hat{\lambda}(u)$ units of negative charge per unit area. The residual is the total charge in the region, the sum of positive and negative charges, which should be approximately zero if the fitted model is correct.

The mean absolute error (MAE) is calculated as the mean of the absolute values of the residuals, and is used to judge the predictive performance of the models. However, when making comparisons across different sample sizes, an alternative to inspecting the MAE of the spatial residuals is to examine the error when using the model to predict the probability of poaching activity. The fitted model is used to make predictions of intensity over the study region W. When using only points in the smaller sampling window B to fit the model, predictions are also made over the larger study region W. Probabilities are then calculated by using the conditional property, $\hat{f}(u) = \hat{\lambda}(u)/\mu_W$. Since the point patterns were generated using probabilities based on poacher environmental preferences, this can be seen as the "observed" probabilities. The error in predicting these probabilities is the difference

between the predicted and observed probability in each grid cell, $e(u) = f(u) - \hat{f}(u)$, where u is the location of each grid cell. The MAE of the probability predictions is calculated as the mean of the absolute errors.

Since maximum likelihood estimation (MLE) is used to estimate parameters, the estimates have approximately a multivariate normal distribution (Baddeley et al., 2015). The Wald statistic to test for zero parameters, $H_0 : \theta_i = 0$, is given by $\hat{\theta}_i / \sqrt{var(\hat{\theta}_i)}$ and has an asymptotic standard normal distribution under the null hypothesis. The Akaike information criterion (AIC) is also based on the likelihood, and can therefore be used for model selection, where the model with the lowest AIC is preferred (Baddeley et al., 2015).

4. Results

Figure 11 shows the MAE of probability predictions when fitting the full covariate model. The boxplots exclude outliers, which only occur beyond the upper whiskers. The MAE is shown for varying sample sizes, for each data generating process. For all data generating process, the variance and error of the probability predictions are reduced as the sample size increases, indicating that the estimates are consistent. The best predictions are made when using the inhomogeneous Poisson, p-thinning, or $p(u)$-thinning processes, since the lowest MAE is obtained for these processes. For $P(u)$-thinning, the mean MAE is slightly larger than for the other thinning processes. The variance is also larger, probably due to the random nature of $P(u)$. The MAE is much lower for the CSR point process, and worst for window sampling. When the model is fitted to data observed in the sampling window, the model does not make good predictions of the probabilities in the larger window.

To examine whether the parameter estimates are consistent, Figure 12 shows boxplots of the coefficients for varying sample sizes when using the full covariate model. Each panel shows one of the covariates. Results are shown for the inhomogeneous Poisson process, but similar results are obtained for the other data generating processes. For all the covariates, the variance of the estimates is reduced as the sample size is increased. The estimates also appear to converge to the mean value as the sample size increases, for all the spatial covariates (the intercept term not included).

Considering the above results, the variance appears to stabilise at a sample size of 200, for all the data generating processes, since only slight improvements are observed when increasing the sample size by 100. Figure 13 shows the distributions, at the sample size of 200, for the number of points $N(\mathbf{x} \cap W)$ in the left panels, and the average intensity $\bar{\lambda}(u)$ in the right panels, for each data generating processes. The black line denotes the distribution of each statistic from the data. For the number of points, the pink line denotes the probability density function for the Poisson distribution, with the sample mean for the parameter λ. In each point process, the Poisson distribution is an excellent fit for the probability density. The sample mean is approximately 200 for all processes, except for the sampling window where it is slightly higher. For the mean intensity, the green line denotes the normal distribution, with sample mean and standard deviation as parameters. The normal distribution appears to be a good fit for the sample distributions. The distributions of the average intensity have the same shape as the number of points, showing that the intensity of the process is proportional to the probability density of the number of points. The intensity of the sampling window process is higher, because it has the same average number of points in a smaller observation window, and is omitted from the boxplot. For all the other processes, the mean is approximately 0.09.

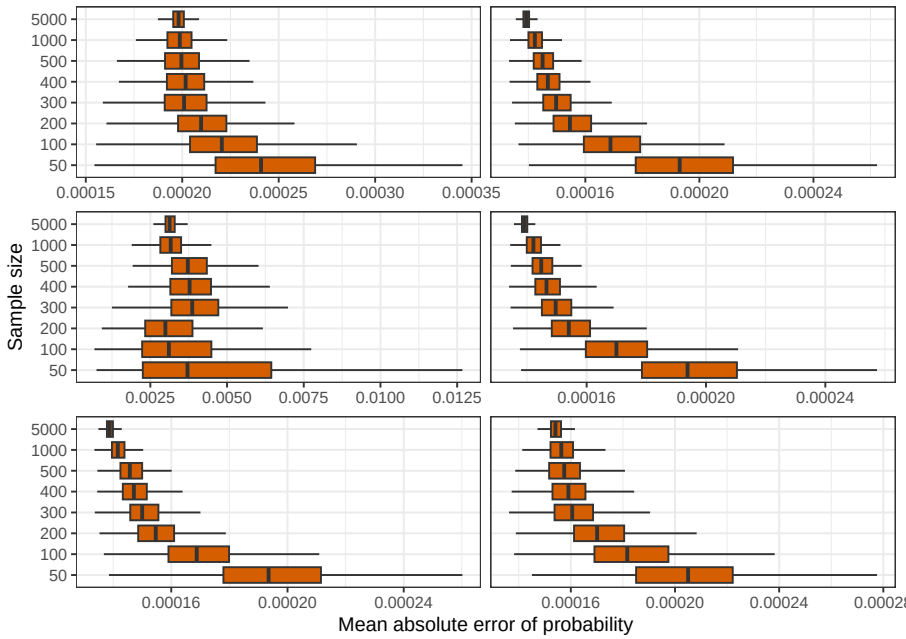

Figure 11. MAE of probability predictions when using the covariate model, for different point processes at varying sample sizes. From left to right, the data generating processes are: *Top row:* CSR and inhomogeneous Poisson. *Middle row:* window sampling and p-thinning. *Bottom row:* $p(u)$-thinning and $P(u)$-thinning.

The MAE of intensity estimates for the covariate model is compared with that of the null model (CSR model), for sample size of 200, in the left panel of Figure 14. The MAE is much lower for the covariate model than the null model for all processes, except for the CSR and $P(u)$-thinning processes, where it is only slightly lower. There are outlying samples with larger MAE in all processes, but this is apparent for both the null and covariate models. The covariate model thus seems to be a reasonable fit to the data. However, collinearity or confounding between the explanatory variables could be present. For example, the effect of the distance to camps or picnic spots covariates on the density of points could possibly be explained by the distance to roads covariate, because both camps and picnic spots are along the roads. Also, gates only occur along the border, so these covariate may also be correlated. Using a subset of the covariates would possibly provide a better fit. The AIC for each model is shown in the right panel of Figure 14, for sample size of 200. The AIC is lower for the full covariate model than the null model, in all the data generating processes, except for the CSR process. The AIC has similar values for all data generating process, except for window sampling, where the AIC is much lower. This could be due to having the same number of expected points as the other processes, but in a much smaller window.

Figure 15 shows the Wald test statistic, at sample size 200, for testing whether the coefficient of a covariate should be zero, in the sampling window and p-thinning processes. The parameters have approximately a multivariate normal distribution. Thus, the test is significant at the 0.05 significance level if the absolute value of the Wald statistic is greater than 1.96. The region between -1.96 and

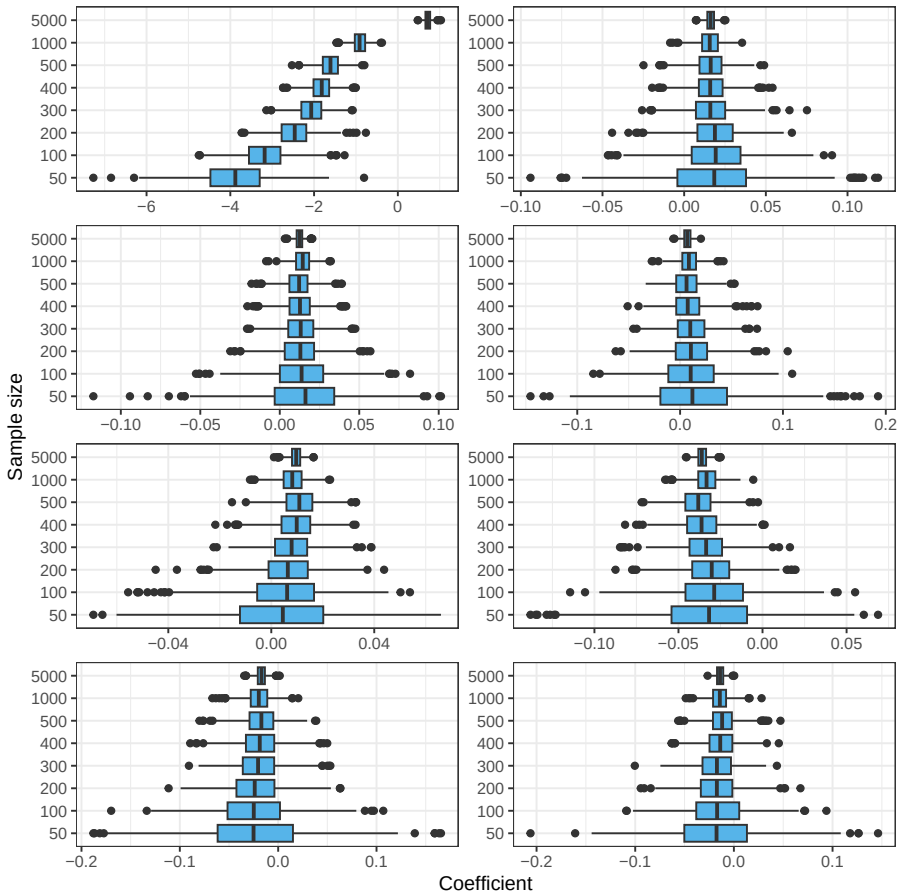

Figure 12. Parameter estimates when using the covariate model, for the inhomogeneous Poisson point process at varying sample sizes. From left to right, the covariates are: *Top row:* Intercept and roads. *Second row:* camps and picnic spots. *Third row:* gates and border. *Bottom row:* dams and watering holes.

1.96 is shaded in grey to visualise the rejection region, the null hypothesis $H_0 : \theta_i = 0$ is rejected outside the grey region. The distance to roads parameter is significantly different from zero for half of the samples in the sampling window process, and nearly half of samples for dams and watering holes. For p-thinning, only the distance to border parameter seems to have a non-zero effect for nearly half of the samples. The poacher probabilities were used in generating the point patterns. They were calculated based on the preferences of the poachers, which were to stay away from roads, camps, picnic spots and gates, and stay near to the border, dams and watering holes. Thus, the intensity should increase as the distance from roads, camps, picnic spots and gates increases, suggesting that these parameters should be greater than zero. Conversely, the intensity should increase as the distance to the border, dams and watering holes decreases, suggesting that these parameters should be less than zero. These relationships appear to hold for the bulk of samples (the boxes, not whiskers), except for

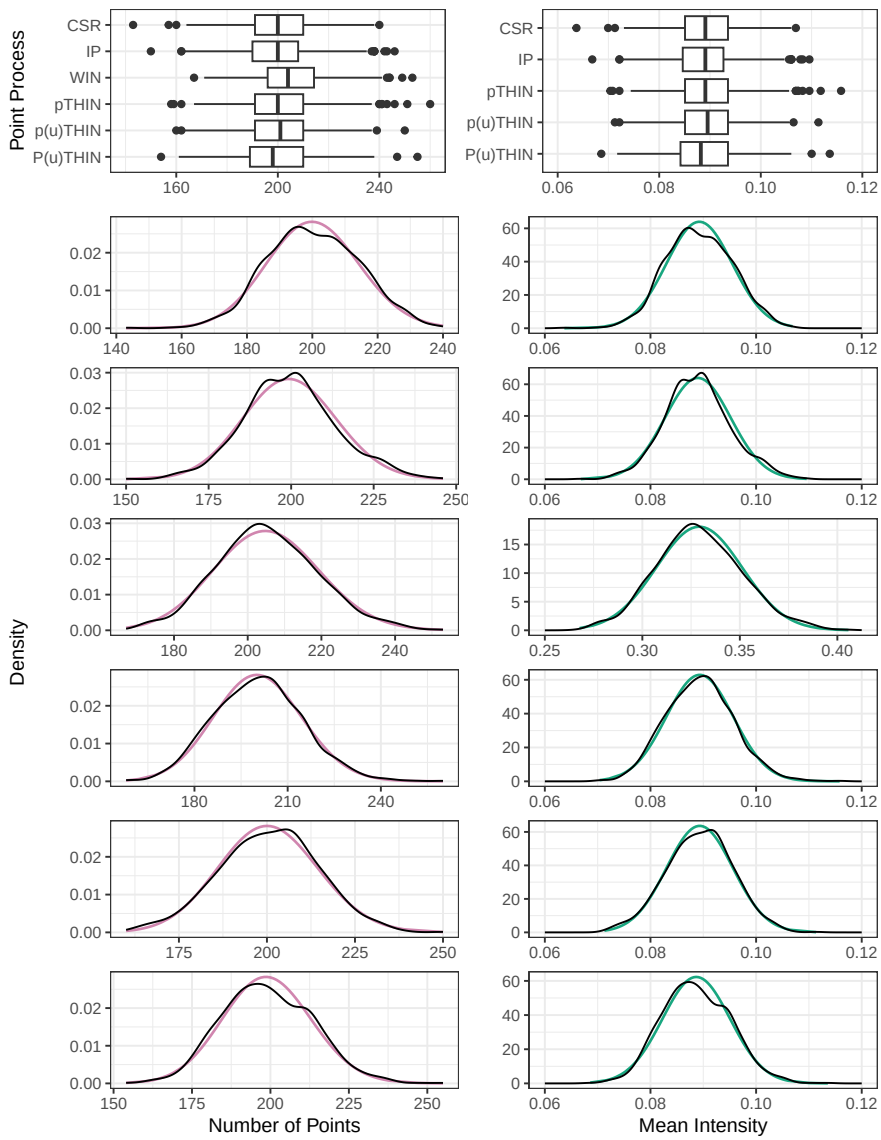

Figure 13. Distributions of the number of points (left) and average intensity (right) for sample size of 200. From top to bottom, the data generating processes are: CSR, inhomogeneous Poisson, window sampling, p-thinning, $p(u)$-thinning, and $P(u)$-thinning.

window sampling, where the parameter for gates is negative and that for the border is positive for half of the samples. This indicates that either some covariates should be removed, or perhaps there is some interaction between covariates.

5. Discussion

The simulation study shows that the full covariate model has similar performance for all data generating processes, except for the CSR and sampling window processes, where the predictions of poacher probability in the large window W are poor. The mean absolute error and parameter estimates appear to be consistent, since the accuracy increases and the variability decreases, when the sample size is increased. The variance seems to stabilise at a sample size of 200, and the simulations show that the number of points has a Poisson distribution, while the average intensity has a normal distribution. The full covariate model does yield lower MAE and AIC than the null model, indicating that the fit is adequate. However, there could be confounding or collinearity present in the full covariate model, and omitting some variables could possibly lead to a better fit.

Other data can also be utilised to improve model. Satellite imagery data, such as that available on Google Earth Engine (Gorelick et al., 2017), can also be used to obtain spatial covariates. Some examples include elevation, slope, normalised difference vegetation index (NDVI), and topographic wetness index (TWI). This data can be collected at different points in time, so that adjustments can be made for seasonal trends. An estimate of the rhino density could also be very useful as a covariate, and could be obtained via aerial photographs (Ferreira et al., 2015). If the analysis is performed only on poached carcasses, rather than all poaching activity, then rhino densities should be used as an exposure variable, and included in the model as an offset term, since poaching events can only occur in regions where there are rhinos. The interest in this paper, is on all areas that poachers utilise, but their presence can only be detected by signs that they leave, which may fade over time. Poachers also hide their snares very well (Gholami, 2018), and make considerable efforts to hide their tracks (Jooste and Park, 2022). The process of detectable poaching activities can thus be seen as a thinned process, since detectable signs do not occur at all of the true poacher locations. Since the environmental factors can impede detection in certain areas, it is like an inhomogeneous process. If a detection rate in all cells can be calculated, then the thinning property can be applied to adjust the model predictions for imperfect detection. The detection of poaching signs also depends on ranger patrols, since the rangers cannot make observations in regions where they have not been. If the duration of patrol in all cells is available, then this can be included in the model as an offset term.

The Poisson point process model given in (5) is similar to the Poisson auto-regression model utilised by Lemieux et al. (2014). However, the latter models the expected number of points, while the former models the average intensity. The intensity model is just as flexible: offset terms can be added to account for exposure, nonlinear relationships can be modelled by including transformed variables, and interactions between variables can be included. However, for the point process model, it may not be necessary to assume that the underlying process is Poisson. If independent $p(u)$-thinning is applied to a non-Poisson point process with intensity $\lambda(u)$, then the resulting process of retained points is approximately inhomogeneous Poisson with intensity $p(u)\lambda(u)$, if $\lambda(u)$ is large and the retention probabilities $p(u)$ are small (Baddeley et al., 2015). Considering the poaching situation in the Kruger National Park, it is reasonable to assume high levels of poaching activity (large λ), and

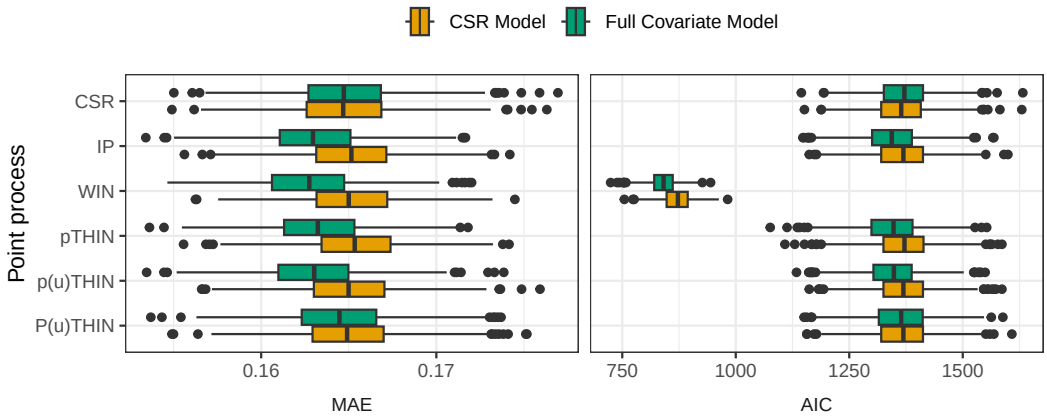

Figure 14. MAE of estimated intensity (left) and AIC (right) of the null model (yellow) and full covariate model (green) for sample size of 200.

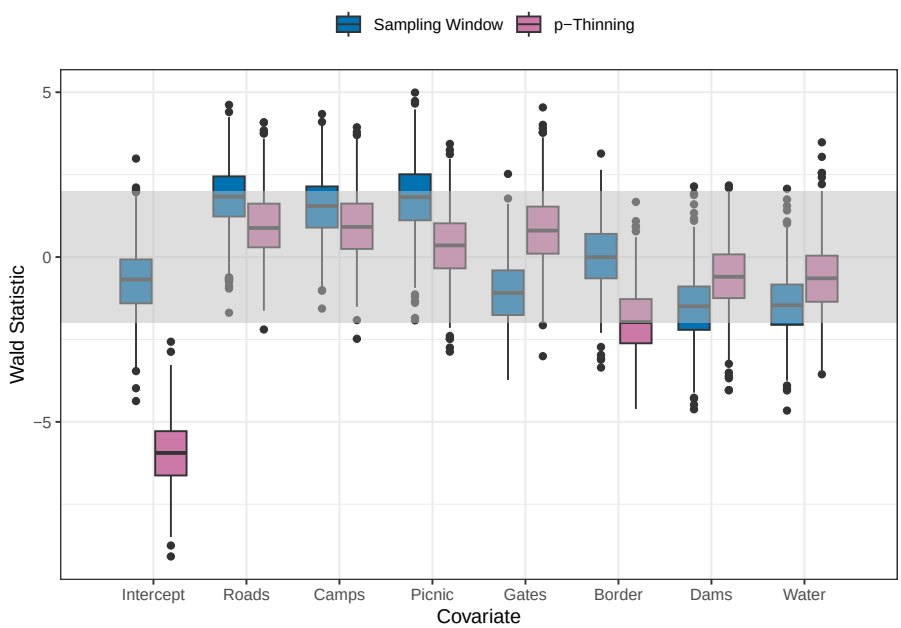

Figure 15. Wald test statistic for zero coefficient in the covariate model for the sampling window and p-thinning processes at sample size of 200.

that only a small proportion of it is detected (small $p(u)$). This means that the Poisson model can be fitted without making any unnecessary assumptions about the underlying distribution of the data. While Poisson models assume spatial independence between points, test statistics and parametric point pattern models are available to detect and account for spatial dependence between points (see Baddeley et al. (2015) for more information). If data is routinely collected over time, then methods for replicated observations can be used (Baddeley et al., 2015). The data points could have marks denoting the season of the observations. Because environmental conditions vary over the seasons, different groups of point patterns could be used for each season. Since favourable results are achieved using point pattern analysis in this work, including temporal information should improve the model.

6. Conclusions

Spatial point process models provide a well-suited method to analyse poaching data within a wildlife park. Since poaching data is not available for this study, the first objective in this paper is to explore different ways to simulate realistic poaching data. The simulations show that an inhomogeneous Poisson point pattern can be obtained either by observing all the points in a region, sampling points in a smaller region, or applying various independent random thinning methods to the entire point pattern. The second objective is to assess the fit of a parametric model to the data. By fitting a simple Poisson model to the data, the spatial covariates can be used to explain the spatial variability in the intensity of the point process. The results suggest that the Poisson point process model, including all the spatial covariates, provides an adequate fit and makes good predictions of the underlying poacher probability, for samples of size 200 and above. If observed data is not available, the heuristic method for calculating poacher probabilities provides a reasonable basis for simulating poaching data. Suggestions for future work include testing results on smaller sample sizes, studying the inter-point interaction using point pattern analysis, application of these methods on real-world data and the comparison of real-world results with other methods applied to the same data.

References

Baddeley, A., Rubak, E., and Turner, R. (2015). *Spatial Point Patterns: Methodology and Applications with R*. Chapman and Hall, New York, NY.

Baddeley, A. and Turner, R. (2005). spatstat: An R package for analyzing spatial point patterns. *Journal of Statistical Software*, **12**, 1–42.

Beale, C. M., Hauenstein, S., Mduma, S., Frederick, H., Jones, T., Bracebridge, C., Maliti, H., Kija, H., and Kohi, E. M. (2018). Spatial analysis of aerial survey data reveals correlates of elephant carcasses within a heavily poached ecosystem. *Biological Conservation*, **218**, 258–267.

Cox, D. R. (1955). Some statistical methods connected with series of events. *Journal of the Royal Statistical Society: Series B (Methodological)*, **17**, 129–157.

Critchlow, R., Plumptre, A., Driciru, M., Rwetsiba, A., Stokes, E. J., Tumwesigye, C., Wanyama, F., and Beale, C. M. (2015). Spatiotemporal trends of illegal activities from ranger-collected data in a Ugandan national park. *Conservation Biology*, **29**, 1458–1470.

Cromsigt, J. P. and te Beest, M. (2014). Restoration of a megaherbivore: Landscape-level impacts of white rhinoceros in Kruger National Park, South Africa. *Journal of Ecology*, **102**, 566–575.

de Matos Dias, D., Ferreguetti, A. C., and Rodrigues, F. H. G. (2020). Using an occupancy approach to identify poaching hotspots in protected areas in a seasonally dry tropical forest. *Biological Conservation*, **251**, 108796.

Di Minin, E., Laitila, J., Montesino-Pouzols, F., Leader-Williams, N., Slotow, R., Goodman, P. S., Conway, A., and Moilanen, A. (2015). Identification of policies for a sustainable legal trade in rhinoceros horn based on population projection and socioeconomic models. *Conservation Biology*, **29**, 545–555.

Diggle, P. J. (2013). *Statistical Analysis of Spatial and Spatio-Temporal Point Patterns*. 3rd edition. Chapman and Hall, CRC Press.

Eloff, C. and Lemieux, A. M. (2014). Rhino poaching in Kruger National Park, South Africa: aligning analysis, technology and prevention. *In Situational Prevention of Poaching*. Routledge, New York, NY, 18–43.

Emslie, R. H. (2020). Ceratotherium simum spp. simum (Southern White Rhino). *The IUCN Red List of Threatened Species*, e.T39317A45814320.

Emslie, R. H., Milliken, T., Talukdar, B., Burgess, G., Adcock, K., Balfour, D., and Knight, M. H. (2018). African and Asian rhinoceroses - status, conservation and trade. CoP18 Doc 83.1 Annex 2. Technical report, CITES Secretariat.

Fang, F., Stone, P., and Tambe, M. (2015). When security games go green: Designing defender strategies to prevent poaching and illegal fishing. *In Proceedings of the 24th International Joint Conference on Artificial Intelligence*. 2589–2595.

Ferreguetti, A. C., Pereira-Ribeiro, J., Prevedello, J. A., Tomas, W. M., Rocha, C. F. D., and Bergallo, H. G. (2018). One step ahead to predict potential poaching hotspots: Modeling occupancy and detectability of poachers in a neotropical rainforest. *Biological Conservation*, **227**, 133–140.

Ferreira, S. M., Ellis, S., Burgess, G., Baruch-Mordo, S., Talukdar, B., and Knight, M. H. (2022). African and Asian rhinoceroses - status, conservation and trade. CoP19 Doc 75 Annex 4. Technical report, CITES Secretariat.
URL: *https://cites.org/sites/default/files/documents/E-CoP19-75.pdf*

Ferreira, S. M., Greaver, C., Knight, G. A., Knight, M. H., Smit, I. P. J., and Pienaar, D. (2015). Disruption of rhino demography by poachers may lead to population declines in Kruger National Park, South Africa. *PLOS ONE*, **10**, 1–18.

Ferreira, S. M., le Roex, N., and Greaver, C. (2019). Species-specific drought impacts on black and white rhinoceroses. *PLOS ONE*, **14**, 1–11.

Gatsheni, B. N. (2019). A Bayesian model for combating poaching of wild life in the Kruger national park. *In Proceedings on the International Conference on Artificial Intelligence. ICAI'19*. 379–384.

Ghoddousi, A., Van Cayzeele, C., Negahdar, P., Soofi, M., Hamidi, A., Bleyhl, B., Fandos, G., Khorozyan, I., Waltert, M., and Kuemmerle, T. (2022). Understanding spatial patterns of poaching pressure using ranger logbook data to optimize future patrolling strategies. *Ecological Applications*, **32**, e2601.

Gholami, S. (2018). Spatio-temporal model for wildlife poaching prediction evaluated through a controlled field test in Uganda. *In 32nd AAAI Conference on Artificial Intelligence, AAAI 2018*.

8012–8013.

Gorelick, N., Hancher, M., Dixon, M., Ilyushchenko, S., Thau, D., and Moore, R. (2017). Google Earth Engine: Planetary-scale geospatial analysis for everyone. *Remote Sensing of Environment*, **202**, 18–27.

Illian, J., Penttinen, A., Stoyan, H., and Stoyan, D. (2007). *Statistical Analysis and Modelling of Spatial Point Patterns*. Wiley.

Jha, A., J, P., and Nameer, P. O. (2022). Contrasting occupancy models with presence-only models: Does accounting for detection lead to better predictions? *Ecological Modelling*, **472**, 110105.

Jooste, J. and Park, T. (2022). *Rhino War*. Pan Macmillan, Johannesbrug.

Kar, D., Fang, F., Fave, F. D., Sintov, N., and Tambe, M. (2015). "A game of thrones": When human behavior models compete in repeated stackelberg security games. *In Proceedings of the 14th International Conference on Autonomous Agents and Multiagent Systems*. 1381–1390.

Kirkland, L. (2023). *A statistical approach to evaluating spatial game theory models for wildlife security*. Phd, University of Pretoria.

Koen, H., De Villiers, J. P., Pavlin, G., De Waal, A., De Oude, P., and Mignet, F. (2014). A framework for inferring predictive distributions of rhino poaching events through causal modelling. *In 17th International Conference on Information Fusion (FUSION)*. IEEE, Salamanca, Spain, 1–7.

Koen, H., Roodt, H., and de Villiers, J. P. (2017). System-level causal modelling of widescale resource plundering: Acting on the rhino poaching catastrophe. *Futures*, **93**, 102–114.

Kuiper, T., Kavhu, B., Ngwenya, N. A., Mandisodza-Chikerema, R., and Milner-Gulland, E. J. (2020). Rangers and modellers collaborate to build and evaluate spatial models of African elephant poaching. *Biological Conservation*, **243**, 108486.

Kulldorff, M. (1997). A spatial scan statistic. *Communications in Statistics - Theory and Methods*, **26**, 1481–1496.

Kulldorff, M., Heffernan, R., Hartman, J., Assunção, R., and Mostashari, F. (2005). A space-time permutation scan statistic for disease outbreak detection. *PLoS medicine*, **2**, 0216–0224.

Lemieux, A. M. (2014). *Situational Prevention of Poaching*. Routledge, New York, NY.

Lemieux, A. M., Bernasco, W., Rwetsiba, A., Guma, N., Driciru, M., and Kulu Kirya, H. (2014). Tracking poachers in Uganda: Spatial models of patrol intensity and patrol efficiency. *In* Lemieux, A. M. (Editor) *Situational Prevention of Poaching*. Routledge, New York, NY, 102–119.

MacFadyen, S., Hui, C., Verburg, P. H., and Van Teeffelen, A. J. A. (2019). Spatiotemporal distribution dynamics of elephants in response to density, rainfall, rivers and fire in Kruger National Park, South Africa. *Diversity and Distributions*, **25**, 880–894.

Park, N., Serra, E., Snitch, T., and Subrahmanian, V. S. (2015). APE: A data-Driven, behavioral model-based anti-poaching engine. *IEEE Transactions on Computational Social Systems*, **2**, 15–37.

PPF (2023). Peace Parks Foundation Open Data Portal.
URL: *https://new-ppfmaps.opendata.arcgis.com/*

R Core Team (2023). R: A Language and Environment for Statistical Computing. Technical report, R Foundation for Statistical Computing, Vienna, Austria.
URL: *https://www.r-project.org*

Rashidi, P., Skidmore, A., Wang, T., Darvishzadeh, R., Ngene, S., and Vrieling, A. (2018). Assessing trends and seasonal changes in elephant poaching risk at the small area level using spatio-temporal Bayesian modeling. *International Journal of Geographical Information Science*, **32**, 622–636.

Rashidi, P., Wang, T., Skidmore, A., Mehdipoor, H., Darvishzadeh, R., Ngene, S., Vrieling, A., and Toxopeus, A. G. (2016). Elephant poaching risk assessed using spatial and non-spatial Bayesian models. *Ecological Modelling*, **338**, 60–68.

Rashidi, P., Wang, T., Skidmore, A., Vrieling, A., Darvishzadeh, R., Toxopeus, B., Ngene, S., and Omondi, P. (2015). Spatial and spatiotemporal clustering methods for detecting elephant poaching hotspots. *Ecological Modelling*, **297**, 180–186.

Rifaie, F., Sugardjito, J., and Fitriana, Y. S. (2015). Spatial point pattern analysis of the Sumatran tiger (Panthera tigris sumatrae) poaching cases in and around Kerinci Seblat National Park, Sumatra. *Biodiversitas Journal of Biological Diversity*, **16**, 311–319.

SADEA (2019). Minister Nomvula Mokonyane highlights progress on the implementation of the Integrated Strategic Management of Rhinoceros and other associated endangered species in SA.
URL: *https://www.environment.gov.za/progressonimplementationofintegratedstrategicmanagementofrhino*

SADEA (2020). Department of Environment, Forestry and Fisheries report back on rhino poaching in South Africa in 2019.
URL: *https://www.environment.gov.za/mediarelease/reportbackon2019_rhinopoachingstatistics*

SADEA (2023). Relentless pressure forces rhino poachers to abandon national parks in 2022, says Creecy.
URL: *https://www.dffe.gov.za/mediarelease/creecy_rhinopoachingupdate2023feb*

SANParks (2017). South African National Parks Annual Report 2016/2017. Technical report, SANParks.
URL: *https://www.sanparks.org/assets/docs/general/annual-report-2017.pdf*

SANParks (2020). South African National Park Data Repository.
URL: *http://dataknp.sanparks.org/sanparks/*

SANParks (2023). South African National Parks Annual Report 2022/2023. Technical report, SANParks.
URL: *https://www.sanparks.org/assets/docs/general/annual-report-2023.pdf*

Shaffer, M. J. and Bishop, J. A. (2016). Predicting and preventing elephant poaching incidents through statistical analysis, gis-based risk analysis, and aerial surveillance flight path modeling. *Tropical Conservation Science*, **9**, 525–548.

Subedi, M. and Subedi, R. (2017). Identification and mapping of risk areas of rhino poaching; a geospatial approach: A case study from eastern sector of Chitwan National Park, Nepal. *Banko Janakari*, **27**, 12–20.

Tango, T. and Takahashi, K. (2005). A flexibly shaped spatial scan statistic for detecting clusters. *International Journal of Health Geographics*, **4**, 1–15. doi:10.1186/1476-072X-4-11/TABLES/6.

Manuscript received 2024-07-29, revised 2025-01-30, accepted 2025-04-10.